https://doi.org/10.5194/amt-2021-340
Preprint. Discussion started: 9 November 2021

Atmospheric Measurement Techniques Discussions

# Variations of Arctic winter ozone from the LIMS Level 3 dataset

Ellis Remsberg[1], Murali Natarajan[1], and Ernest Hilsenrath[2]

[1]Science Directorate, NASA Langley Research Center, 21 Langley Blvd, Mail Stop 401B, Hampton, VA 23681, USA

[2]Fellow at Joint Center for Earth System Technology, University of Maryland at Baltimore County, 1000 Hilltop Circle, Baltimore, MD 21250, USA

Correspondence to: Ellis Remsberg (ellis.e.remsberg@nasa.gov)

https://doi.org/10.5194/amt-2021-340
Preprint. Discussion started: 9 November 2021

Atmospheric Measurement Techniques Discussions

**Abstract**

The Nimbus 7 limb infrared monitor of the stratosphere (LIMS) instrument operated from October 25, 1978, through May 28, 1979. Its Version 6 (V6) profiles and their Level 3 or zonal Fourier coefficient products have been characterized and archived in 2008 and in 2011, respectively. This paper focuses on the value and use of daily ozone maps from Level 3, based on a gridding of its zonal coefficients. We present maps of V6 ozone on pressure surfaces and compare them with several rocket-borne chemiluminescent ozone measurements that extend into the lower mesosphere. Daily, synoptic maps of V6 ozone and temperature illustrate that they are an important aid in interpreting satellite limb-infrared emission versus local measurements, especially when they occur during dynamically active periods of northern hemisphere winter. We then show a sequence of V6 maps of upper stratospheric ozone, spanning the minor stratospheric warmings of late January and early February 1979. The map sequence of V6 geopotential height reveals how ozone was changing in the vortex and at the centers of adjacent anticyclones. We also report on zonal variations of the tertiary ozone maximum of the upper mesosphere and its associated temperature fields during winter. These several examples provide a guide to researchers for further exploratory analyses of middle atmosphere ozone from LIMS.

## 1 Introduction and objectives

The historic Nimbus 7 Limb Infrared Monitor of the Stratosphere (LIMS) experiment provided data on middle atmosphere ozone from October 25, 1978, through May 28, 1979, for scientific analysis and for comparisons with atmospheric models (Gille and Russell, 1984). Ozone is an excellent tracer of middle atmosphere transport processes at high latitudes. As an early example, Leovy et al. (1985) showed how daily maps of the LIMS ozone fields correlate well with geopotential height (GPH) fields on the 10-hPa pressure surface. They also reported on the rapidly changing effects of wave activity on ozone, which led to a better understanding of stratospheric transport processes within models. Hitchman et al. (1989) also analyzed the temperature fields from LIMS and reported on Arctic observations of an elevated stratopause in late autumn to early winter that they associated with momentum forcings from gravity waves.

https://doi.org/10.5194/amt-2021-340
Preprint. Discussion started: 9 November 2021

Atmospheric Measurement Techniques
Discussions

Current research is focusing on the 3-dimensional character of ozone in the upper stratosphere and mesosphere, based on more recent satellite datasets. Several studies report on how temperature and ozone vary in association with sudden stratospheric warming (SSW) events (de la Camara et al., 2018; Kim et al., 2020; Shams et al., 2021). Manney et al. (1995) and Harvey et al. (2008) report on the development of low ozone pockets (LOPs) in the region of the Aleutian anticyclone during winter. Siskind et al. (2005; 2021) report on the occurrence of a mesospheric cooling associated with SSWs and on the role of gravity waves for modeling ozone in the upper mesosphere. Chandran et al. (2013) developed a climatology of the Arctic elevated stratopause. Sofieva et al. (2021) analyzed a multiyear dataset for regional trends in stratospheric ozone since 2001. LIMS provides similar data on ozone from an earlier decade for further comparisons.

The LIMS profiles have been retrieved with an improved Version 6 (V6) algorithm. Those V6 (or Level 2) profiles were archived in 2008 and include ozone, temperature, and GPH that extend from 316 hPa to ~0.01 hPa. The co-located V6 profiles of water vapor ($H_2O$), nitric acid vapor ($HNO_3$), and nitrogen dioxide ($NO_2$) extend through the stratosphere. Lieberman et al. (2004) analyzed the V6 temperature profiles and found evidence for non-migrating tides, due to the interaction of the diurnal tide and planetary zonal-wave 1, especially in late January 1979. Holt et al. (2010) analyzed the descent of V6 $NO_2$ from the lower mesosphere to within the polar stratospheric vortex, where it interacts with ozone. Remsberg et al. (2013) assimilated V6 ozone profiles in a reanalysis model and gained improved estimates of column ozone, especially in Arctic winter. Such reanalysis studies assimilate temperature and ozone profiles within a model framework. However, the models only approximate the effects of small-scale variations, so it is also useful to consider observed variations of the LIMS parameters without resort to a model. Keep in mind that smaller-scale atmospheric variations also contribute to the analyzed intermediate and large-scale fields from V6. This paper provides some examples of the larger-scale variations of Arctic ozone, temperature, and GPH.

https://doi.org/10.5194/amt-2021-340
Preprint. Discussion started: 9 November 2021

Atmospheric Measurement Techniques Discussions

The SPARC Data Initiative (SPARC-DI) includes monthly zonal averages for the chemical species from V6 (see Tegtmeier et al., 2013; SPARC, 2017; and Remsberg et al., 2021). In Section 2 we show January zonal averages of V6 ozone and temperature profiles that extend even higher or to near the mesopause. The V6 Level 3 (map) product provides a 3-dimensional context for those zonal mean data. Daily V6 maps are also an aid in interpretating individual V6 profiles versus correlative data, especially during dynamically disturbed periods. Specifically, in Section 3 we compare several nighttime V6 ozone profiles with those obtained with a rocket-borne chemiluminescent (CHEM) technique (Hilsenrath et al., 1980). Those profile comparisons are for December 15 and for January 27 and 28, when the temperature and ozone fields were affected by planetary wave forcings. There is a corresponding cooling and variations of ozone in the winter lower mesosphere associated with the warming in the upper stratosphere. Section 4 presents variations of ozone and GPH at northern extratropical latitudes during the minor SSW events of late January and early February 1979, as a complement to the more comprehensive findings of Harvey et al. (2008) on the occurrence of LOPs within anticyclones based on solar occultation satellite data. Section 5 gives some details on the variability of the tertiary ozone maximum in the upper mesosphere during that same period, as an adjunct to the monthly zonal average values reported by Smith et al. (2018). Section 6 considers the variability of V6 ozone within the lowermost extratropical stratosphere, but also cautions users about occasional, pseudo-ozone features in the tropics. Section 7 concludes that the V6 Level 3 product represents an important resource for further studies of the effects of transport and chemistry of middle atmosphere ozone.

## 2 Characteristics of V6 Level 3 data

### *2.1 LIMS measurements and analyses*

Nimbus 7 was in a near-polar orbit, and LIMS made measurements at ~1 pm local time along its ascending (A or south-to-north) orbital segments and at ~11 pm on its descending (D or north-to-south) segments. A-D time differences are of the order of 10 hours at most all latitudes because LIMS viewed the atmosphere 146.5° clockwise of the spacecraft velocity vector, as seen from above, or 33.5° counterclockwise from its negative velocity vector. The A-D differences narrow from 10 to about 6 hours from 60°N to 80°N, due to the orbital geometry of Nimbus 7. The V6

https://doi.org/10.5194/amt-2021-340
Preprint. Discussion started: 9 November 2021

Atmospheric Measurement Techniques
Discussions

processing algorithm accounts for low-frequency spacecraft motions that affect the LIMS view of the horizon. As a result, its measured radiance profiles are registered well in pressure-altitude (Remsberg et al., 2004). Retrieved V6 ozone, temperature, and GPH profiles extend from 316 hPa to ~0.01 hPa and have a vertical point spacing of ~0.88 km with an altitude resolution of ~3.7 km. They occur every ~1.6 degrees of latitude along orbits, and LIMS made measurements with a duty cycle of about 11 days on and 1 day off over its planned observing lifetime. The LIMS algorithms (Remsberg et al., 2007) do not account for non-local thermodynamic equilibrium (NLTE) effects in ozone (Solomon et al., 1986; Mlynczak and Drayson, 1990) and in $CO_2$ (Edwards et al., 1996; Manuilova et al., 1998), so there are positive biases in the retrieved V6 ozone throughout the mesosphere during daylight. However, the V6 nighttime ozone is essentially free of NLTE effects below about the 0.05-hPa level.

A sequential-estimation (SE) algorithm generated daily, zonal Fourier coefficients (zonal mean and up to 6-wavenumber, sine and cosine values) for Level 3 at every 2° of latitude and at up to 28 vertical levels (Remsberg and Lingenfelser, 2010). The V6 SE algorithm uses better estimates of data uncertainty and a shorter relaxation time of ~2.5 days for the zonal wave coefficients, as compared with the earlier algorithm of Remsberg et al. (1990). The SE analysis is also insensitive to the very few large, unscreened ozone profiles values found in the lower stratosphere, as noted in Remsberg et al. (2013, their Fig. 1a). The SE algorithm combines the coefficients from both the A and D orbital segments and effectively interpolates the profile data in time to provide a continuous, 216-day set of daily zonal coefficients versus pressure-altitude for each of the retrieved LIMS parameters. Those combined (A+D) Level 3 coefficients are the basis for a gridding of synoptic maps at 1200Z of ozone and related parameters. Note that Level 3 also contains coefficients from its separate A and D profiles; their 'zonal mean' values correspond to the local time-of-day of their respective measurements. The Level 3 data are in ASCII format for easy access and use.

### *2.2 Monthly average V6 data*

https://doi.org/10.5194/amt-2021-340
Preprint. Discussion started: 9 November 2021

Atmospheric Measurement Techniques
Discussions

One can generate monthly average distributions from the daily Level 3 files of temperature, GPH, and species (ozone, $H_2O$, $HNO_3$, and $NO_2$); zonal averages for the V6 species were supplied to the SPARC Data Initiative or SPARC-DI (SPARC, 2017; Hegglin et al., 2021). Tegtmeier et al. (2013) compared the V6 monthly ozone distributions with ones from other satellite-based limb sensors and reported good agreement throughout the stratosphere. Although the species cross sections of SPARC-DI (2017) extend only up to the 0.1-hPa level (~64 km), V6 average ozone extends higher or to about 0.015 hPa (~75 km). Figure 1 shows the latitude-pressure cross section for January from just the descending (D) orbital profiles, which avoids the NLTE biases from the daytime ozone. Stratospheric ozone mixing ratios in Fig. 1 have largest values at about 10 hPa near the Equator (> 9.2 ppmv), and they decrease sharply above and below that level. Maximum mixing ratios for the middle to high latitudes occur between 3 to 5 hPa, due to the larger zenith angles and longer paths of the ultraviolet light for production of atmospheric ozone. There is a nighttime ozone minimum of ~1.2 ppmv across most latitudes of the middle mesosphere. A tertiary ozone maximum is present in the upper mesosphere near the day/night terminator zones of the LIMS measurements for January (~50°S and ~65°N), in accordance with the interpretation of Marsh et al. (2001). The location (~0.02 hPa) and magnitude (~3.5 ppmv) of the NH maximum agree with those reported from subsequent satellite studies by Smith et al. (2018, their Fig. 4). On the other hand, while the V6 ozone poleward of ~60°S is also from descending orbital profiles, it corresponds to daylight conditions at the high southern latitudes in January. Thus, the decrease of mesospheric V6 ozone at 0.1 hPa and poleward of 60°S in Fig. 1 indicates merely a change from night to day values.

Radiances from two 15-µm $CO_2$ channels are used for retrievals of V6 temperature versus pressure or T(p), and they are also free of NLTE effects below about the 0.05-hPa level (~70 km) (Lopez-Puertas and Taylor, 2001). Retrievals for T(p) in the stratosphere account for the effects of horizontal temperature gradients to first order. Single profile errors for T(p) range from 1 K at 10 hPa to greater than 2 K in the upper mesosphere. Systematic errors from T(p) are the primary source of bias error for ozone, which grow to of order 16% in the middle mesosphere (Remsberg et al., 2021, Table 1). As a complement to the V6 ozone of Fig. 1, we show the descending (~nighttime) V6 T(p) distribution for January in Figure 2, which extends to near the 0.01-hPa

https://doi.org/10.5194/amt-2021-340
Preprint. Discussion started: 9 November 2021



level. The large-scale features of the T(p) distribution compare well with climatological values from the late 1970s (Fleming et al., 1990), having a maximum value of about 285 K at the high latitude, SH stratopause and minimum values of < 200 K at the tropical tropopause and near the summer mesopause. There is also an apparent elevation of the Arctic zonal-average stratopause.

Figure 3 shows average, zonal (wave) standard deviations (SD) about the daily zonal mean of the combined-mode (A+D) V6 ozone for January, where the SD values are also part of the LIMS SPARC-DI product. There are relatively small SD values at low latitudes from 7 to 10 hPa; it is assumed that they are a result of both Kelvin and gravity wave activity. Effects of more vigorous, planetary wave activity are most apparent at high northern latitudes throughout the stratosphere and in the upper mesosphere. Ozone shows little zonal variation in the SH upper stratosphere of Fig. 3, due to constraints on the upward propagation of waves through the summer zonal easterlies. SD values near the tropical tropopause are due mostly to residual effects of emissions from thin cirrus and represent spurious ozone variations (see Section 6).

## 3. V6 comparisons with rocket-borne chemiluminescent ozone measurements

In this section we consider V6 comparisons with three nighttime, rocket-borne ozone soundings using the CHEM technique of Hilsenrath (1980)—one at White Sands, NM, (32.4°N, 253.5°E) on December 15, 1978, and two more at Poker Flat, AK, (65.1°N, 212.5°E) on the successive days of January 27 and 28, 1979. Estimated total error for CHEM ozone is 14% (precision plus accuracy), according to Hilsenrath and Kirschner (1980).

Ozone comparisons for December 15 are in Figure 4, where the four V6 profiles are spaced about 2.6° in latitude along the descending orbital segment with the LIMS instrument viewing in the NNW direction. The short-dashed V6 profile is at 29.2°, and the long-dashed profile is at 37.2°. The location of the rocket ozone sounding lies midway between them. Horizontal bars on the profiles are estimates of ozone error; they overlap between V6 and CHEM, except in the upper stratosphere. However, the corresponding V6 polar ozone map at 4.6 hPa reveals a region

https://doi.org/10.5194/amt-2021-340
Preprint. Discussion started: 9 November 2021



of elevated ozone near White Sands (blue dot) on that date. Note that while zonal variations in the polar plot are from a gridding (2° latitude and 5.625° longitude) of the Level 3 coefficients, there is no smoothing of the gridded field in the meridional direction; there is good continuity across latitudes, nonetheless. The CHEM profile is a local measurement and has a vertical resolution that ranges from 1.5 km at 60 km to 0.1 km at 20 km; the nearby V6 profiles have a lower vertical resolution of ~3.7 km and are an average over the finite horizontal length (~300 km or ~3° latitude) of the LIMS tangent layer. Thus, an ozone field that varies in both space and time may lead to a somewhat reduced quality for comparisons between the localized rocket and limb-viewing satellite profiles in Fig. 4.

Because V6 ozone is obtained from retrievals of the measured V6 ozone radiance profiles, the LIMS retrieved temperature profile must be representative of the atmospheric state for the forward model of ozone radiance. Figure 5 shows the corresponding temperature comparisons between V6 and the correlative rocket Datasonde instrument (*). Agreement between them is very good throughout the upper stratosphere, which means that the retrieved V6 ozone is nearly unaffected by temperature bias error. Temperatures do not agree as well in the lowermost mesosphere. The map of V6 temperature in Fig. 5 clearly indicates that there are significant variations in the temperature field at 0.68 hPa near 35°N on December 15. Still, there is little evidence of disagreement between V6 and CHEM ozone in Fig. 4 at 0.68 hPa, indicating that the temperature variations are determined well along the LIMS view path for the forward radiance calculations of ozone.

The two late January comparisons occurred at the time of a stratospheric, zonal wave-1 warming event and during a time of advection of air from lower latitudes to near the Pole (Leovy et al., 1985). Figure 6 shows three co-located V6 ozone profiles from along a nearby descending orbital segment at ~2204Z (nighttime). The LIMS instrument was viewing from its sub-satellite location of 80.5°N, 130°E, and the CHEM rocket launch was two hours earlier or at 2005Z; there is good agreement for ozone between them, even in the mesosphere. A second rocket launch followed at 0833Z of the next day. Since the V6/CHEM ozone and T(p) comparisons are similar for the two days, we show results for January 27 only. The CHEM sonde recorded two ozone

https://doi.org/10.5194/amt-2021-340
Preprint. Discussion started: 9 November 2021

Atmospheric Measurement Techniques Discussions

maxima, one at about 0.6 hPa and another near 15 hPa, and the V6 profiles of Fig. 6 also have maxima at those levels plus an ozone minimum at about 3 hPa. Agreement is good between the profiles, although the CHEM profile has more vertical structure. The ozone maximum at about 15 hPa is primarily due to advection of ozone of higher mixing ratios from lower latitudes just prior to the warming event. Leovy et al. (1985) provide a more detailed discussion of the advective changes for ozone in the middle stratosphere during January 1979.

Figure 7 shows the V6 temperature profile comparisons; T(p) from the Datasonde also has more vertical structure, as expected from a localized measurement. Although there is significant horizontal structure in the temperature field surrounding Poker Flat, the V6 temperature profiles agree reasonably with the Datasonde values and indicate that retrieved V6 ozone again has very little bias due to temperature. T(p) values reach a maximum of order 250 K at about 3 to 4 hPa, or where the ozone profiles in Fig. 6 reveal a relative minimum within a low-ozone pocket (LOP) that extends to other levels or from about 7 hPa to 2 hPa.

The polar vortex is located over northern Europe and Asia on January 27; it is shifted off the Pole because of effects from large-scale, planetary waves on the development of SSWs (Andrews et al., 1987, Chapter 6). The polar vortex region has low ozone and relatively cold temperatures; stratospheric temperatures over Alaska have a relative maximum (the SSW). The sounding rocket profile from Poker Flat occurs near the center of an anticyclone and in the region of relatively low ozone.

Figure 8 shows that there is concurrent cooling at 0.46 hPa or above the Alaskan anticyclone, and the corresponding nighttime (or D) ozone field exhibits a local maximum at that same level. Conversely, there is a major temperature increase in the Arctic region above the polar stratospheric vortex over northern Europe, where ozone values remain relatively low. Since ozone is an excellent tracer of transport processes in Arctic winter, it can reveal dramatic changes with altitude, associated with this SSW event. In summary, Figs. 4 through 8 show the utility of daily maps from LIMS Level 3 for the validation and interpretation of the ozone fields

https://doi.org/10.5194/amt-2021-340
Preprint. Discussion started: 9 November 2021



during dynamically disturbed conditions. In the next section, we consider sequences of polar plots of both GPH and ozone from January 27 through February 17, 1979, to illustrate the value of the V6 Level 3 products for studies of ozone transport over time.

## 4. Variations of upper stratospheric ozone during stratospheric warmings

Manney et al. (1995) and Harvey et al. (2004, 2008) contain comprehensive analyses about the occurrence of polar anticyclones and their associated LOPs from analyses of GPH and ozone fields from several different satellites. They determined the extent and character of the polar vortex based on meteorological data from the UK Met Office and as obtained from relatively low, vertical resolution radiance profiles from operational, nadir temperature sounders. Those meteorological analyses extend through the stratosphere but only up to the lower mesosphere. The V6 GPH coefficients extend through both the stratosphere and mesosphere, as derived from the V6 T(p) profiles that have a vertical resolution of order 3.7 km. Thus, the LIMS dataset offers potentially more detail about the occurrence of LOPs.

The first panel of Figure 9 shows a map of NH GPH at 4.6 hPa on January 27 for comparison with the ozone map in Fig. 6 and the temperature map in Fig. 7. Lowest ozone values are in the polar vortex, which is asymmetric about the Pole. A second, relatively low value of ozone (or LOP) is associated with the anticyclone over the Alaskan sector. One can determine horizontal winds from gradients of GPH on the 4.6-hPa surface and thereby estimate the transport of ozone to first order. Qualitatively, the direction and strength of the large-scale transport follows from the character of the cyclonic and anticyclonic features on the GPH map. A large-scale cyclonic circulation about the vortex transports air from middle latitudes to across the Pole on January 27.

The other three panels of Figure 9 are a sequence of three daily NH maps of GPH from February 3 to February 17; each successive map is spaced one week from the previous one. This sequence shows that both the vortex and anticyclone weaken during the three weeks following January 27

https://doi.org/10.5194/amt-2021-340
Preprint. Discussion started: 9 November 2021



at this level. The vortex is re-centered on the Pole on February 17, and the anticyclone is nearly absent at this level following the two minor warming events.

The map sequence in Fig. 9 also indicates that there are significant changes in the horizontal transport of ozone during this dynamically active period. Morris et al. (1998) conducted model calculations to show that there can be chemical changes of ozone in the upper stratosphere at that time. Ozone reactions are affected by changes with latitude in solar insolation, temperature, and $NO_x$. As an example, Figure 10 (top left) is a map of the V6 descending (nighttime) $NO_2$ on January 27, and it shows that air having larger $NO_2$ values was transported northward from middle latitudes toward the anticyclone. Thus, it is likely that there is some loss of ozone due to reactions with $NO_x$ (and $NO_2$) in the middle stratosphere that is contributing to the LOP feature. The other three panels of Figure 10 show the evolution of ozone for February 3 through 17, following that of January 27 (in Fig. 6). Based on the GPH panels of Fig. 9, there was a deepening of the LOP from January 27 to February 3, but a filling of it thereafter. Transport of air from middle to higher latitudes decreased from February 3 to February 17, when the vortex and anticyclone weakened. But the anticyclone also weakened from January 27 to February 3. Thus, a chemical loss of ozone due to $NO_x$ may also have occurred during that first week. Although we do not show a sequence of maps for other levels, the V6 Level 3 product indicates significant variations in ozone, temperature, GPH, and $NO_2$ throughout the upper stratosphere.

## 5. Variations of the tertiary ozone maximum

Smith et al. (2018) describe the changing monthly, zonally averaged character of the wintertime tertiary ozone maximum of the polar upper mesosphere. They point out that the low latitude edge of the tertiary ozone maximum is where $HO_x$ radicals and the chemical loss of ozone due to reactions with them are reduced. The Level 3 ozone and temperature products provide daily, 3-dimensional information about those processes. The top two panels of Figure 11 are of upper mesospheric ozone on the 0.022-hPa surface (~72 km) for January 13 and February 10, respectively. The bottom two panels show the variations of temperature on those same days. First, consider the two ozone plots, which are from only the descending (or nighttime) orbital

https://doi.org/10.5194/amt-2021-340
Preprint. Discussion started: 9 November 2021

Atmospheric Measurement Techniques Discussions

segments. V6 ozone radiance profiles have low signal-to-noise in the upper mesosphere; the precision estimate for retrieved ozone and its Fourier coefficients is 0.32 ppmv at 0.022 hPa. Therefore, we show gridded ozone maps in Fig. 11 based on just the zonal mean and the sine and cosine coefficients for waves 1 and 2. Elevated values of ozone occur at a lower latitude on January 13 than on February 10, which is consistent with the slightly different location of the terminator on those two days. One can also see that the tertiary maximum has a larger value on February 10 than on January 13.

The bottom two panels of Fig. 11 are maps of temperature for January 13 and February 10, respectively, for comparison with the ozone fields. The temperature maps are gridded from the zonal mean and coefficients out to zonal wavenumber 6. There is significant zonal structure in them, and temperatures are much warmer in the Canadian sector on January 13 than on February 10. There are meridional gradients of temperature on both days. On January 13 there is also a well-defined mesospheric vortex (not shown), and the highest values of ozone correlate reasonably with it; by February 10 the vortex was disturbed at this level. Recall that there were two minor warmings and associated lower mesospheric cooling events during late January and early February. It is very likely that there were wave-driven disturbances in the upper mesosphere during that time, due to filtering of gravity waves and their dissipation (e.g., Siskind et al. 2005). We infer that the warmer temperatures of mid-January at this level led to a radiative relaxation and a descent of relatively dry air into the vortex region. A reduction in water vapor will mean that there are fewer $HO_x$ radicals for the destruction of ozone near the terminator zone, leading to an accumulation of ozone by February 10. Although the seasonal evolution of the tertiary ozone maximum is understood reasonably well (Smith et al., 2018), there is more information about this ozone feature from the daily maps of ozone, T(p), and GPH from Level 3.

## 6. V6 ozone in the lowermost stratosphere

Significant exchanges of air and ozone occur from the extratropical stratosphere to the troposphere in winter and spring (Gettelman et al., 2011). Figure 3 also showed that there are large zonal variations about the daily zonal means of ozone in the Arctic region of the lower

https://doi.org/10.5194/amt-2021-340
Preprint. Discussion started: 9 November 2021



stratosphere. There are similar variations in GPH (and derived winds) and in zonal wave activity that lead to ozone transport. Zonal variations are resolved in the daily ozone maps down to the 146-hPa level. In fact, Shepherd et al. (2014) integrated the V6 monthly zonal mean ozone above the tropopause and subtracted it from observed total ozone, as part of their assessment of long-term trends of tropospheric ozone from models. Their calculation of extratropical tropospheric ozone based on LIMS agrees with that obtained from other ozone datasets.

There is also a relative excess of SD ozone values in Fig. 3 centered at 68 hPa at tropical latitudes, and similar anomalies occur in other LIMS months, too (not shown). As an example, Figure 12 shows an ozone map at 68 hPa (~18 km) for the correlative measurement day of December 15, 1978, to give more insight about the source of the tropical variations. Ozone mixing ratio values in Fig. 12 are of order 2 to 3 ppmv at high latitudes, becoming much smaller in the subtropics. However, there is also an unexpected high value of 2 to 3 ppmv at about 15°N, 150°E. Limb measurements in the ozone channel include radiance effects from cirrus particles that can occur along the view path, although the retrieved ozone mixing ratio profiles were screened of those effects to first order (Remsberg et al., 2007). Even so, we note that ozone is easily affected by any excess radiance because of highly non-linear effects for retrievals of ozone from the radiances in the lower stratosphere. It is very likely that the anomalous ozone at 68 hPa is a result of residual effects from subvisible cirrus, which is nearly ubiquitous over the western tropical Pacific region (see SPARC, 2006, Fig. 1.8).

While individual V6 ozone profiles may include such spurious features in the tropics, the Level 3 ozone product at 68 hPa is affected mainly when there is organized convection and outflow of air that persist for several days. The adjacent map of tropical ozone at 46 hPa appears unperturbed (not shown), and tropical ozone at 100 hPa approaches zero. There are much smaller anomalies in maps of nitric acid, as its mixing ratio retrieval is very nearly linear. Anomalies are not present in maps of V6 $H_2O$ at 68 hPa because the cloud screening algorithm for $H_2O$ accounts for the larger vertical field-of-view and extent over altitude for the measurements of the water vapor channel of LIMS. To summarize, one must be mindful that the Level 3 product may show pseudo ozone at 68 hPa in the tropics, but likely not in the extratropics.

https://doi.org/10.5194/amt-2021-340
Preprint. Discussion started: 9 November 2021

Atmospheric Measurement Techniques
Discussions

## 7. Conclusions on the utility of LIMS V6 Level 3 ozone

This report provides guidance to researchers for their use of the LIMS V6 Level 3 product and their generation of daily gridded distributions of its temperature, ozone, and GPH on pressure surfaces. $H_2O$, $NO_2$, and $HNO_3$ are also available for the stratosphere from the Level 3 product. The V6 dataset represents an early baseline for considering changes in the middle atmosphere from 1979 to today and into the future. Atmospheric concentrations of the greenhouse gases (GHG), $CO_2$, $CH_4$, and CFCs, were smaller in 1979 versus now. As an example, the LIMS algorithm for retrieving T(p) profiles is based on a middle stratosphere $CO_2$ value of 327 ppmv, compared with ~415 ppmv in 2021. As a result, middle atmosphere T(p) distributions were warmer in 1979, which affects both the chemistry and transport of ozone. LIMS also made measurements at a time when stratospheric effects from volcanoes were minimal and when catalytic effects of chlorine on ozone were relatively small. Accordingly, Stolarski et al. (2012) found small, but significant changes in the distribution of upper stratospheric ozone for recent decades compared with 1978-1979.

The LIMS measurements in the winter Arctic region occurred when there was a lot of wave activity for the transport and mixing of ozone. Ozone varies dramatically in winter, particularly during times of stratospheric warming events. There was a so-called Canadian warming in early December 1978, two minor SSW events in late January and early February, and a final warming in late February 1979. We showed V6 comparisons with temperature and ozone profile data obtained using rocket-borne chemiluminescent (CHEM) techniques, and we pointed out how an examination of changes in their nearby fields are essential for the interpretation and validation of V6 profiles against correlative measurements. The Level 3 dataset provides daily details on those variations in latitude, longitude, and altitude, along with related variations in temperature, geopotential height, and $NO_2$. We noted also that there are instances of spurious, excess ozone from the Level 3 coefficients at 68 hPa in the tropics but not in the extratropical stratosphere. One may find that there are regional changes in ozone in recent decades compared with that in 1978-1979 from V6 (see, e.g., Sofieva et al., 2021).

Atmospheric Measurement Techniques Discussions

V6 nighttime ozone is accurate up through the middle mesosphere, and surface maps of the large-scale variations of ozone are relatively accurate through the upper mesosphere. Daily ozone and temperature maps reveal zonal wave features in the region of the wintertime, tertiary ozone maximum of the upper mesosphere. Together with V6 maps of T(p) and GPH, one may explore the daily evolution of that ozone maximum throughout the NH winter of 1978-1979.

**Data Availability**

The LIMS V6 Level 3 product is at the NASA EARTHDATA site of EOSDIS and its website: https://disc.gsfc.nasa.gov/datacollection/LIMSN7L3_006.html (Remsberg et al., 2011). The SPARC-Data Initiative data are located at https://doi.org/10.5281/zenodo.4265393 (Hegglin et al., 2021). We acknowledge the individual instrument teams and respective space agencies for making their measurements available, and the Data Initiative of WCRP's (World Climate Research Programme) SPARC (Stratospheric Processes and their Role in Climate) project for organizing and coordinating the compilation of the chemical trace gas datasets used in this work.

*Author Contributions.* ER wrote the manuscript and prepared the figures with contributions from his co-authors. EH provided his rocketsonde data on ozone and temperature along with their error estimates.

*Competing interests*. The authors declare no competing interests for this study.

*Acknowledgements*. The authors appreciate John Gille and Jim Russell III and members of the LIMS Science Team for their leadership in the development of the LIMS instrument and on the processing of its historic data products. The authors are grateful to John Burton, Praful Bhatt, Larry Gordley, B. Thomas Marshall, and R. E. Thompson for producing the V6 Level 2 dataset. They acknowledge Gretchen Lingenfelser for her work in generating and archiving the V6 Level 3 coefficient dataset. They also thank V. Lynn Harvey for her comments on a draft version of

https://doi.org/10.5194/amt-2021-340
Preprint. Discussion started: 9 November 2021


Atmospheric Measurement Techniques Discussions

the manuscript. EER and MN carried out their work while serving as Distinguished Research Associates of the Science Directorate at NASA Langley.

https://doi.org/10.5194/amt-2021-340
Preprint. Discussion started: 9 November 2021

Atmospheric Measurement Techniques Discussions

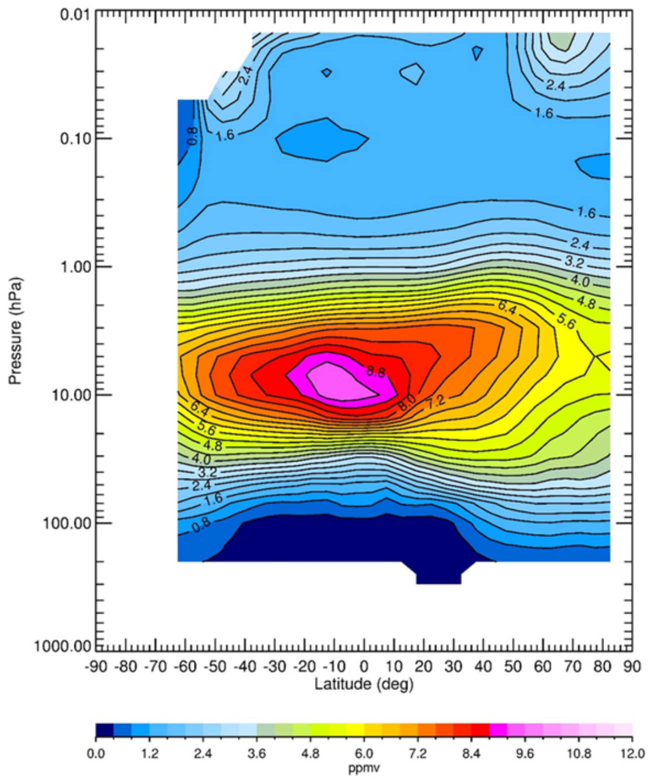


Figure 1—LIMS V6 Level 3 monthly zonal mean ozone for descending-mode only (or nighttime equatorward of ~55°S) for January 1979. Contour interval (CI) is 0.4 ppmv.

https://doi.org/10.5194/amt-2021-340
Preprint. Discussion started: 9 November 2021


Atmospheric Measurement Techniques
Discussions

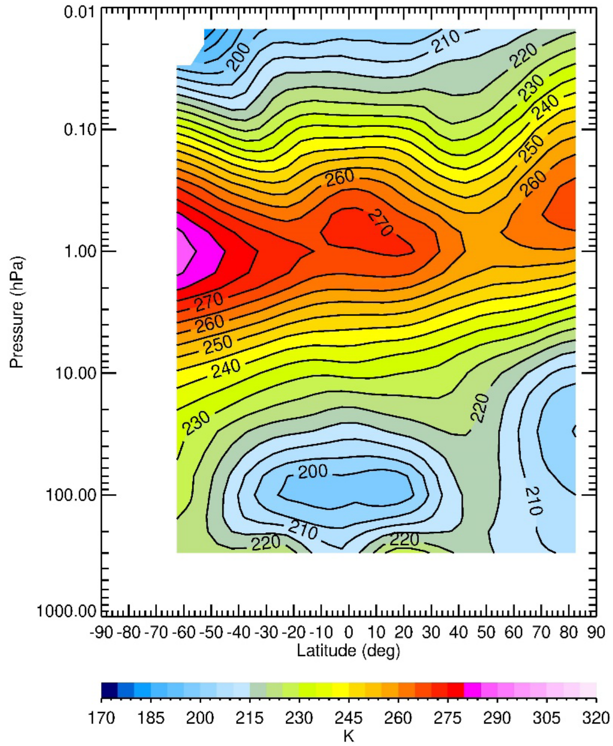


Figure 2—Zonal average, descending-mode, temperature for January 1979. CI is 5 K.

https://doi.org/10.5194/amt-2021-340
Preprint. Discussion started: 9 November 2021


Atmospheric Measurement Techniques
Discussions

437

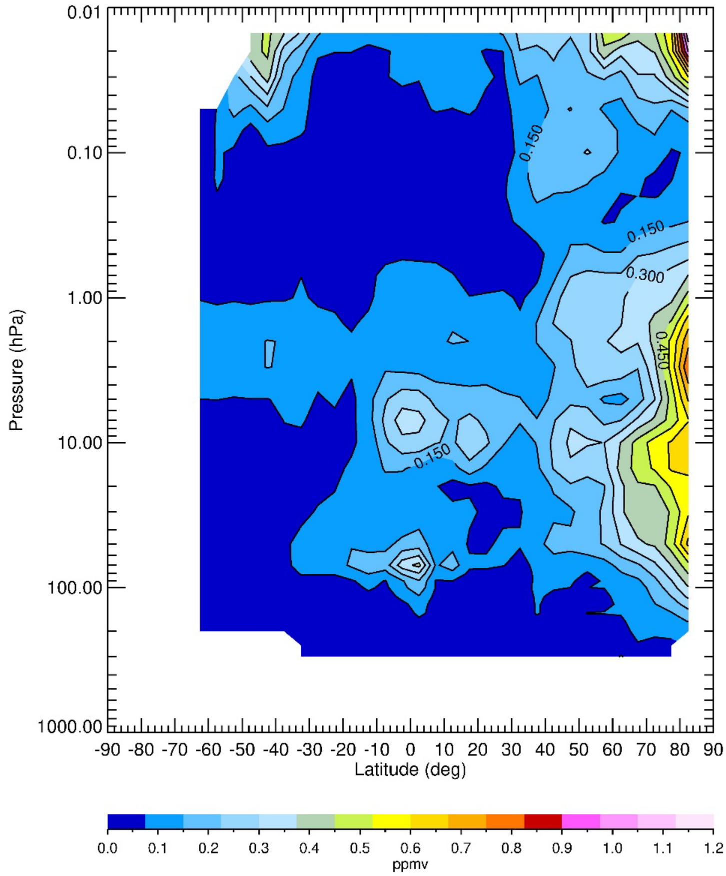


438

439 Figure 3—Zonal standard deviation about the average of (A+D) ozone for January 1979.

440 Contour interval is 0.075 ppmv.

441

https://doi.org/10.5194/amt-2021-340
Preprint. Discussion started: 9 November 2021

Atmospheric Measurement Techniques Discussions

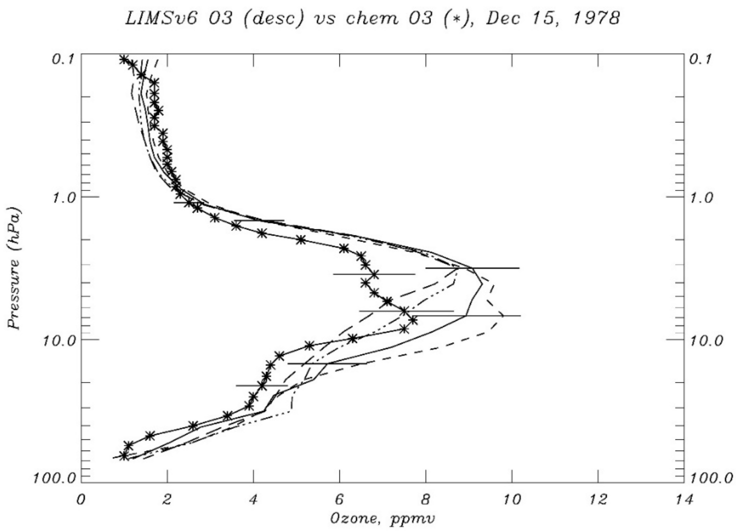


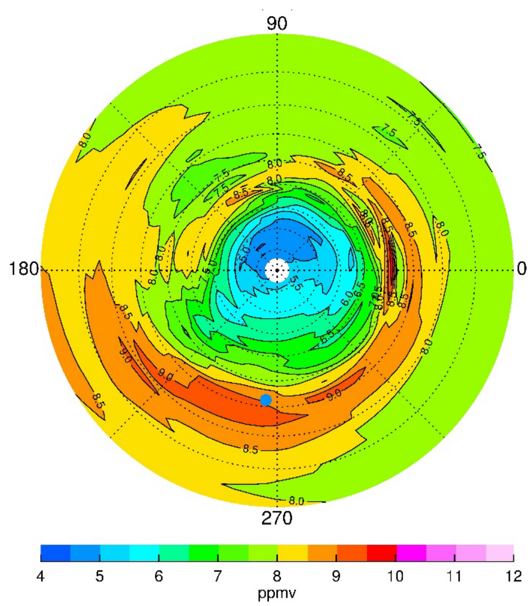


Figure 4—(top) Profiles of V6 ozone compared with CHEM sonde ozone (*) on December 15. The four V6 profiles are separated by about 2.5° latitude on the descending orbit. Horizontal bars are estimates of ozone error. (bottom) NH V6 ozone distribution at 4.6 hPa; Greenwich (0°E) is at right, and contour interval (CI) is 0.5 ppmv. Latitudes (dotted circles) are spaced every 10°. The blue dot denotes White Sands.

https://doi.org/10.5194/amt-2021-340
Preprint. Discussion started: 9 November 2021

Atmospheric Measurement Techniques Discussions
Open Access

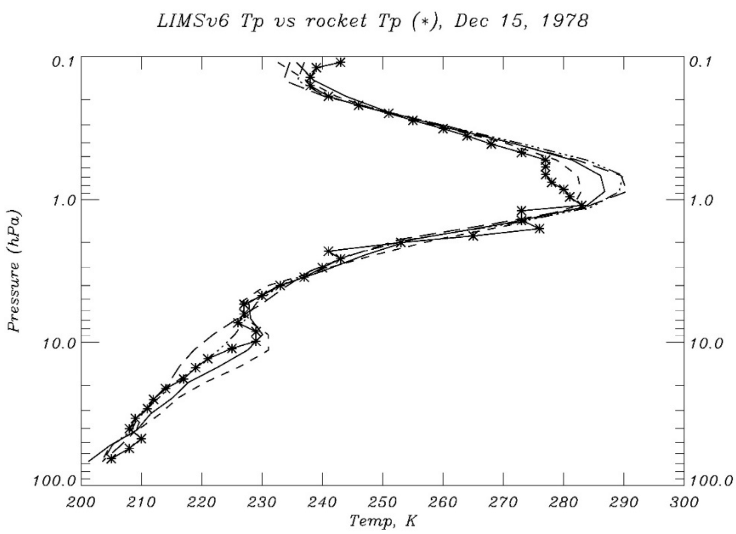


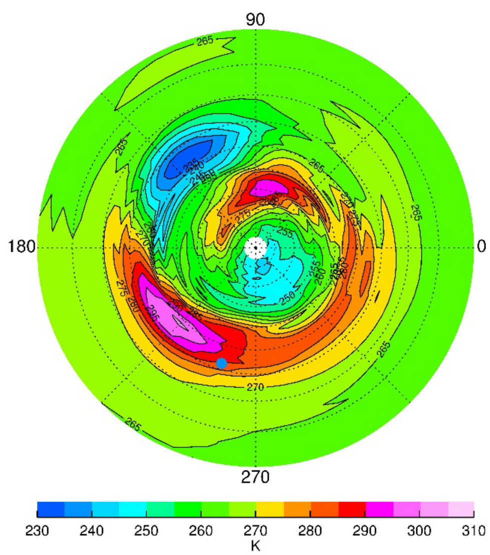


Figure 5—(top) Profiles of V6 temperature compared with Datasonde values (*) on December 15. The four V6 profiles are separated as in Fig. 4, where the short-dashed curve is for 29.2° and the long-dashed curve is for 37.2°. (bottom) NH V6 temperature distribution at 0.68 hPa; contour interval is 5 K, and blue dot denotes White Sands.

https://doi.org/10.5194/amt-2021-340
Preprint. Discussion started: 9 November 2021

Atmospheric Measurement Techniques Discussions

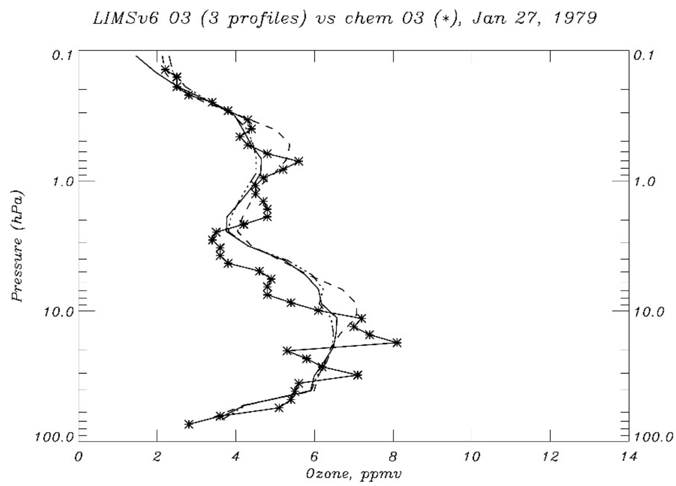


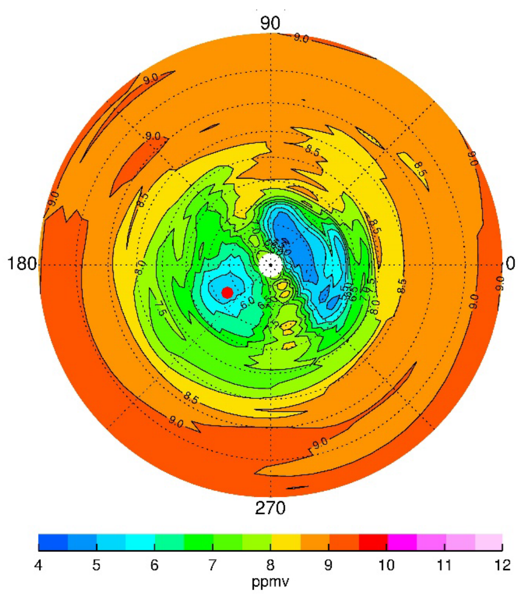


Figure 6—(top) As in Fig. 4, but for January 27, 1979, at Poker Flat, AK (65°N, 212.5°E); (bottom) NH V6 distribution of ozone at 4.6 hPa; CI is 0.5 ppmv and red dot is Poker Flat.

https://doi.org/10.5194/amt-2021-340
Preprint. Discussion started: 9 November 2021

Atmospheric Measurement Techniques
Discussions

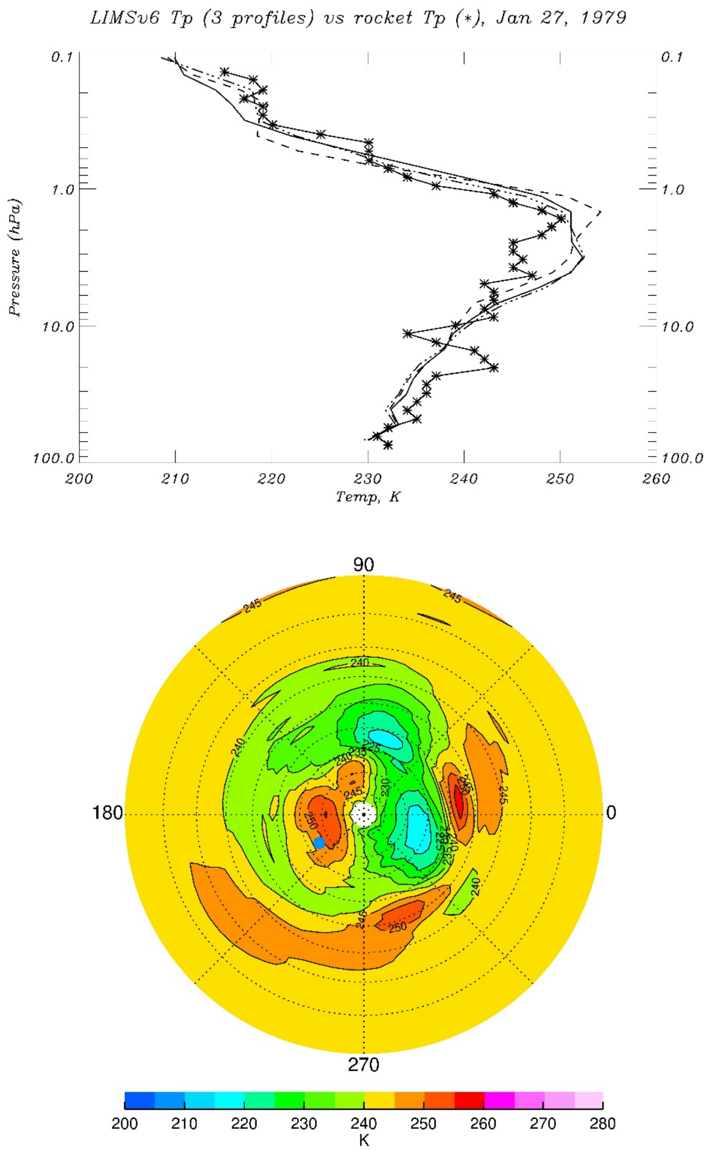


Figure 7—(top) As in Fig. 5, but for January 27, 1979. (bottom) NH V6 temperature at 4.6 hPa on January 27; Contour interval is 5 K. Blue dot is location of Poker Flat.

https://doi.org/10.5194/amt-2021-340
Preprint. Discussion started: 9 November 2021

Atmospheric Measurement Techniques
Discussions

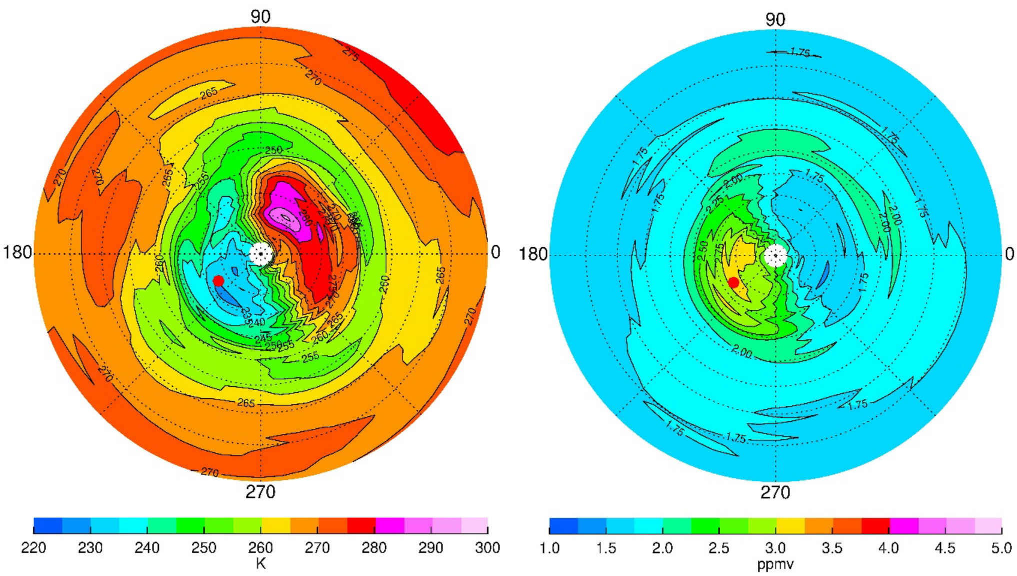


Figure 8---—(left) Temperature at 0.46 hPa for January 27, 1979, for comparison with Fig. 7. (right) Ozone at 0.46 hPa for comparison with Fig. 6. Contour interval for T(p) is 5 K and for ozone is 0.25 ppmv. Red dot is location of Poker Flat.

https://doi.org/10.5194/amt-2021-340
Preprint. Discussion started: 9 November 2021




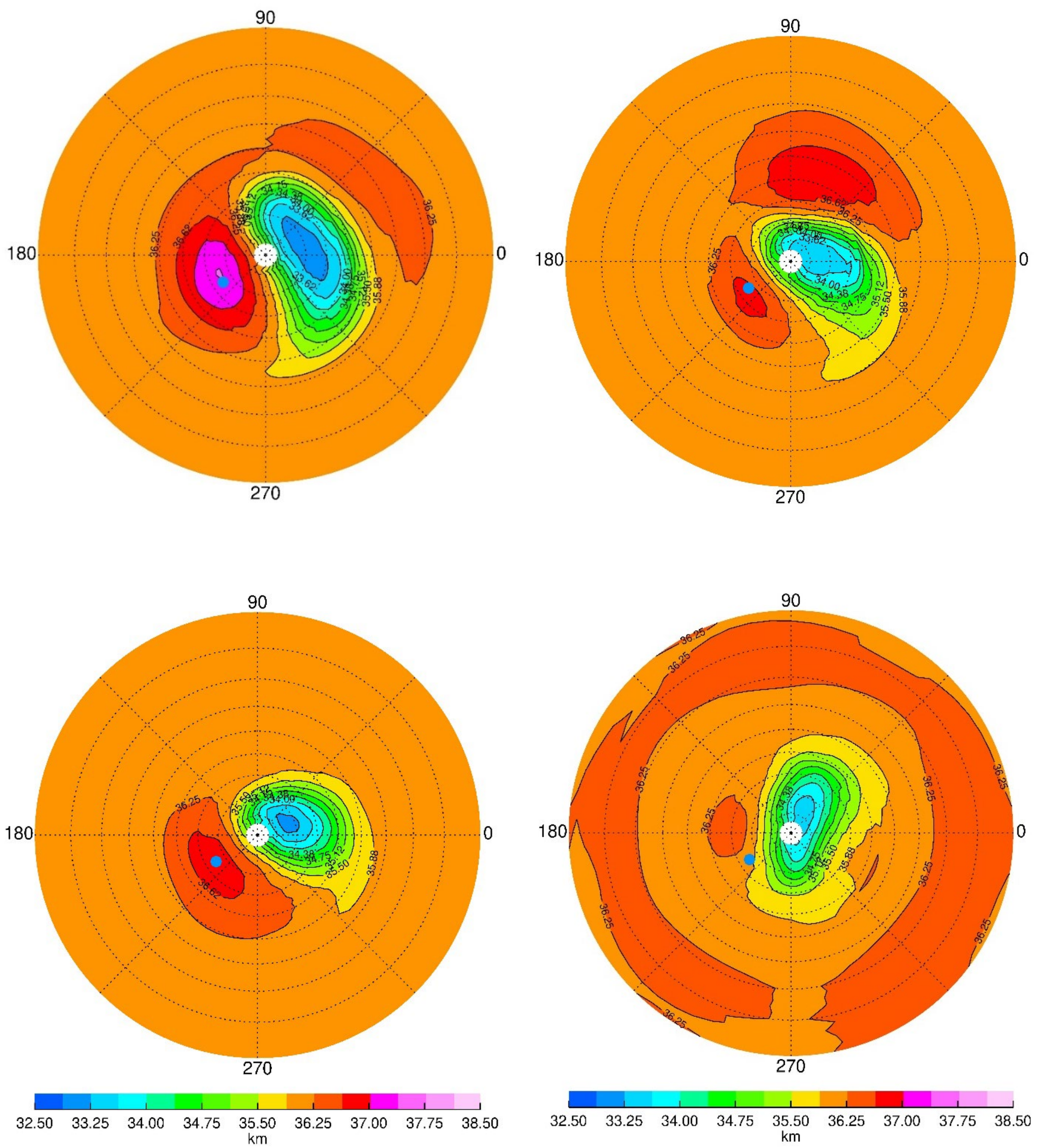


Figure 9-- NH V6 GPH at 4.6 hPa; contour interval (CI) is 0.375 gpkm. Blue dot is location of Poker Flat. Panels are spaced one week apart; (top left) January 27; (top right) February 3; (bottom left) February 10; and (bottom right) February 17.

https://doi.org/10.5194/amt-2021-340
Preprint. Discussion started: 9 November 2021

Atmospheric Measurement Techniques
Discussions

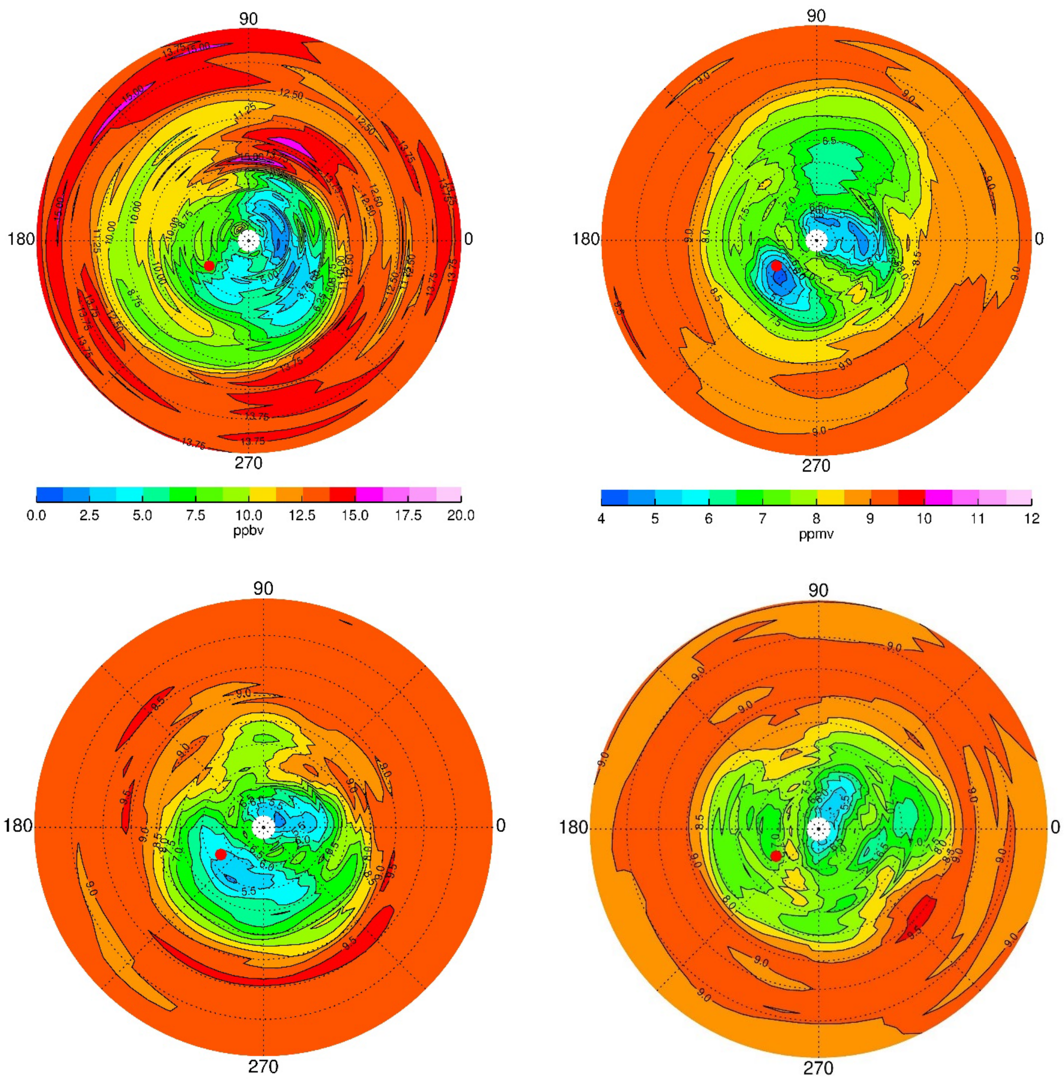


Figure 10—Maps for 4.6 hPa of (top left) nighttime $NO_2$ on January 27, CI is 1.25 ppbv and red dot is Poker Flat; (top right) ozone on February 3; (bottom left) ozone on February 10; and (bottom right) ozone on February 17; CI is 0.5 ppmv. Ozone color bar applies to the bottom two panels, as well.

https://doi.org/10.5194/amt-2021-340
Preprint. Discussion started: 9 November 2021


Atmospheric Measurement Techniques
Discussions
Open Access

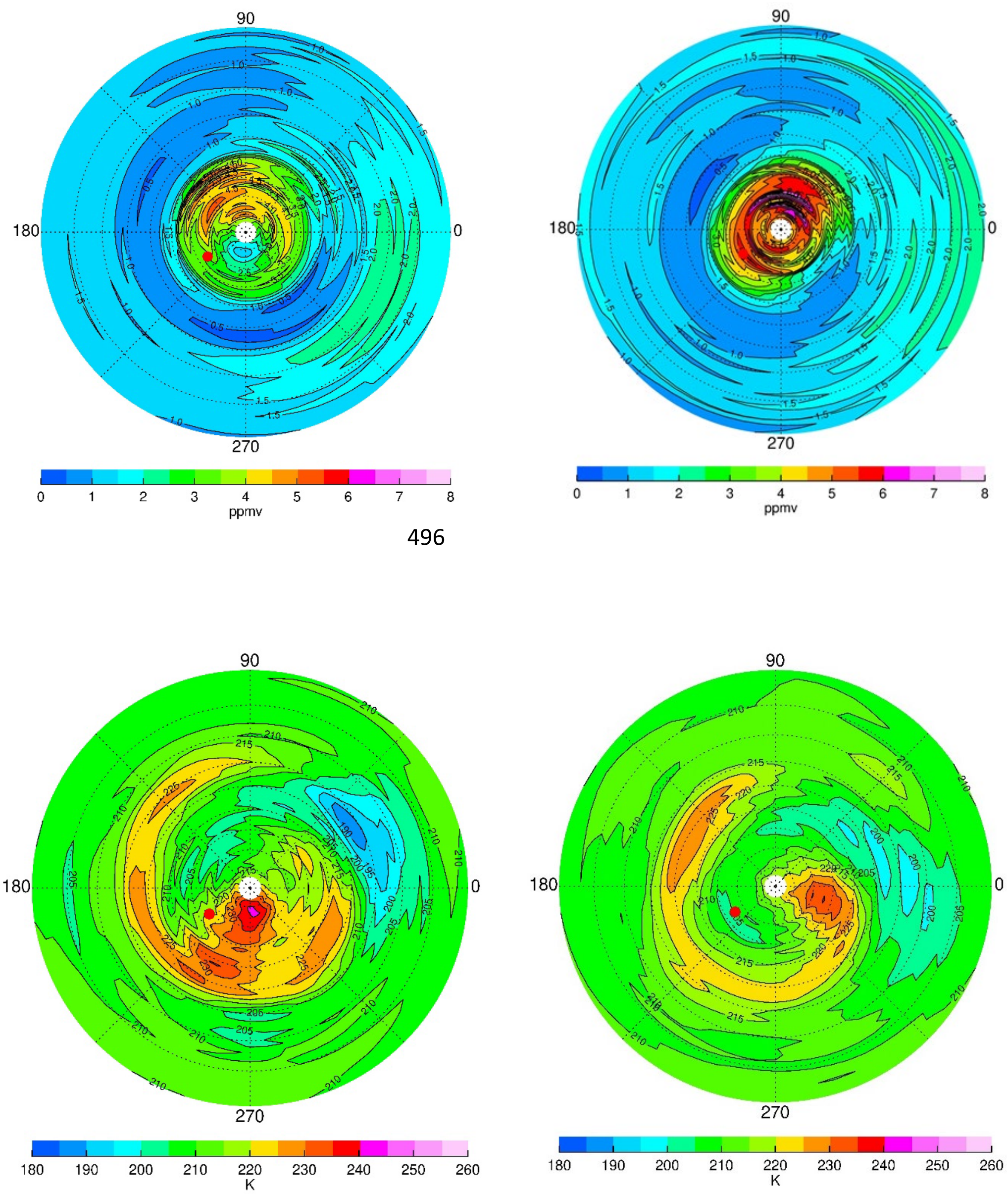


Figure 11—(top) Distributions of NH ozone at 0.022 hPa on January 13 (left) and February 10 (right), respectively; contour interval is 0.5 ppmv. (bottom) NH temperature at 0.022 hPa on January 13 (left) and February 10 (right); contour interval is 5 K.

https://doi.org/10.5194/amt-2021-340
Preprint. Discussion started: 9 November 2021

Atmospheric Measurement Techniques Discussions

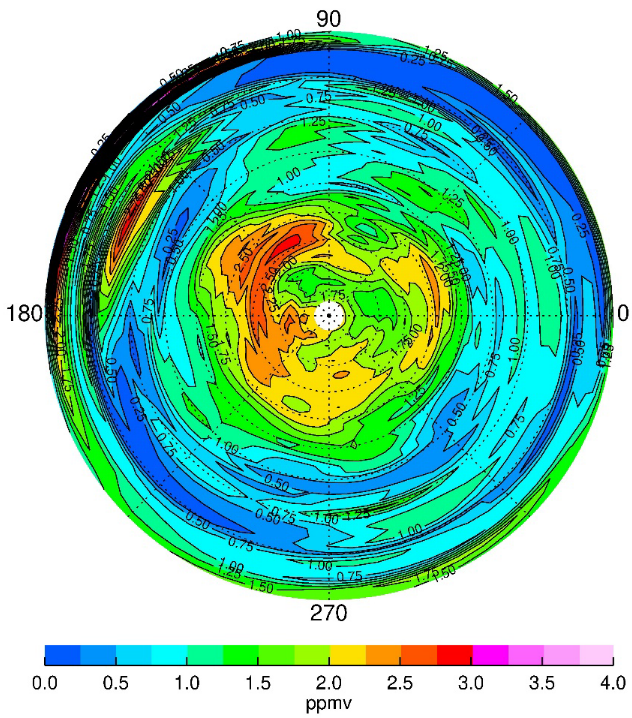


Figure 12—NH V6 ozone distribution at 68 hPa for December 15, 1978. Contour interval is 0.25 ppmv.

References

Andrews, D. G., Holton, J. R., and Leovy, C. B.: *Middle Atmosphere Dynamics*, 1st Ed., 489 pp., Academic Press, 1987.

Chandran, A., Collins, R. L., Garcia, R. R., Marsh, D. L., Harvey, V. L., Yue, J., and de la Torre, L.: A climatology of elevated stratopause events in the whole atmosphere community climate model, J. Geophys. Res. Atmos., 118, 1234-1246, https://doi.org/10.1002/jgrd.50123, 2013.

de la Cámara, A., Abalos, M., Hitchcock, P., Calvo, N., and Garcia, R. R.: Response of Arctic ozone to sudden stratospheric warmings, Atmos. Chem. Phys., 18, 16499–16513, https://doi.org/10.5194/acp-18-16499-2018, 2018.

Edwards, D. P., Kumer, J. B., Lopez-Puertas, M., Mlynczak, M. G., Gopalan, A., Gille, J. C., and Roche, A.: Non-local thermodynamic equilibrium limb radiance near 10 µm as measured by UARS CLAES, J. Geophys. Res., 101, D21, 26,577-26,588, https://doi.org/10.1029/96JD02133, 1996.

Fleming, E.L., Chandra, S., Barnett, J. J., and Corney, M.: Zonal mean temperature, pressure, zonal wind, and geopotential height as functions of latitude, COSPAR International Reference Atmosphere: 1986, Part II: Middle Atmosphere Models, Adv. Space Res., 10 (12), 11-59, https://doi.org/10.1016/0273-1177(90)90386-E, 1990.

Gettelman, A., Hoor, P., Pan, L. L., Randel, W. J., Hegglin, M. I., and Birner, T.: The extratropical upper troposphere and lower stratosphere, Rev. Geophys., 49, RG3033, https://doi.org/10.1029/2011RG000355, 2011.

Gille, J. C. and Russell III, J. M.: The limb infrared monitor of the stratosphere: experiment description, performance, and results, J. Geophys. Res., 84, 5125-5140, https://doi.org/10.1029/JD089iD04p05125, 1984.

Harvey, V. L., Pierce, R. B., Hitchman, M. H., Randall, C. E., and Fairlie, T. D.: On the distribution of ozone in stratospheric anticyclones, J. Geophys. Res., 109, D24308, https://doi:10.1029/2004JD004992, 2004.

Harvey, V. L., Randall, C. E., Manney, G. L., and Singleton, C. S.: Low-ozone pockets observed by EOS-MLS, J. Geophys. Res., 113, D17112, https://doi.org/10.1029/2007JD009181, 2008.

Hegglin, M. I., Tegtmeier, S., Anderson, J., Bourassa, A. E., Brohede, S., Degenstein, D., Froidevaux, L., Funke, B., Gille, J., Kasai, Y., Kyrola, E. T., Lumpe, J., Murtagh, D., Neu, J. L., Perot, K., Remsberg, E. E., Rozanov, A., Toohey, M., Urban, J., von Clarmann, T., Walker, K. A., Wang, H-J.., Arosio, C., Damadeo, R., Fuller, R. A., Lingenfelser, G., McLinden, C., Pendelbury, D., Roth, C., Ryan, N. J., Sioris, C., Smith, L., and Weigel, K.: Overview and update of the SPARC Data Initiative: comparison of stratospheric composition measurements from satellite limb sounders, Earth Syst. Sci. Data, 13, 1855-1903, https://doi.org/10.5194/essd-1855-2021, 2021.

Hilsenrath, E.: Rocket observations of the vertical distribution of ozone in the polar night and during a mid-winter stratospheric warming, Geophys. Res. Lett., 7, 581-584, https://doi.org/10.1029/GL007i008p00581, 1980.

Hilsenrath, E., and Kirschner, P. T.: Recent assessment of the performance and accuracy of a chemiluminescent rocket sonde for upper atmospheric ozone measurements, Rev. Sci. Instrum., Vol. 51, 1381-1389, https://doi.org/10.1063/1.1136080, 1980.

Hitchman, M. H., Gille, J. C., Rodgers, C. D., and Brasseur, G.: The separated polar winter stratopause: a wave driven climatological feature, J. Atmos. Sci., 46, 410-422, https://doi.org/10.1175/1520-0469(1989)046%3C0410:TSPWSA%3E2.0.CO;2, 1989.

Holt, L. A., Randall, C. E., Harvey, V. L., Remsberg, E. E., Stiller, G. P., Funke, B., Bernath, P. F., and Walker, K. A., Atmospheric effects of energetic particle precipitation in the Arctic winter 1978–1979 revisited, J. Geophys. Res., 117, D05315, https://doi.org/10.1029/2011JD016663, 2012.

Kim, J-H., Jee, G., Choi, H., Kim, B-M., and Kim, S-J.: Vertical structures of temperature and ozone changes in the stratosphere and mesosphere during stratospheric sudden warmings, J. Astron. Space Sci., 37, 69-75, https://doi.org/10.5140/JASS.2020.37.1.69, 2020.

Leovy, C. B., Sun, C-R., Hitchman, M. H., Remsberg, E. E., Russell, III, J. M., Gordley, L. L., Gille, J. C., and Lyjak, L. V.: Transport of ozone in the middle stratosphere: evidence for planetary wave breaking, J. Atmos. Sci., 42, 230-244, https://doi.org/10.1175/1520-0469(1985)042%3C0230:TOOITM%3E2.0.CO;2, 1985.

Lieberman, R. S., Oberheide, J., Hagan, M. E., Remsberg, E. E., and Gordley, L. L.: Variability of diurnal tides and planetary waves during November 1978–May 1979, J. Atmos. Solar-Terr. Phys., 66, 517–528, https://doi.org/10.1016/j.jastp.2004.01.006, 2004.

Lopez-Puertas, M. and Taylor, F. W.: Non-LTE Radiative transfer in the Atmosphere, World Scientific Publ. Co., River Edge, NJ, USA, 504 pp., 2001.

Manney, G. L., Froidevaux, L., Waters, J. W., Zurek, R. W., Gille, J. C., Kumer, J. B., Mergenthaler, J. L., Roche, A. E., O'Neill, A., and Swinbank, R.: Formation of low-ozone pockets in the middle stratospheric anticyclone during winter, J. Geophys. Res. Atmos., 100, 13939-13950, https://doi.org/10.1029/95JD00372, 1995.

Marsh, D., Smith, A., Brasseur, G., Kaufmann, M., and Grossmann, K.: The existence of a tertiary ozone maximum in the high-latitude middle mesosphere, Geophys. Res. Lett., 28, 4531-4534, https://doi.org/10.1029/2001GL013791, 2001.

Manuilova, R. O., Gusev, O. A., Kutepov, A. A., von Clarmann, T., Oelhaf, H., Stiller, G. P, Wegner, A., Lopez-Puertas, M., Martin-Torres, F. J., Zaragoza, G., and Flaud, J.-M.: Modelling of non-LTE limb spectra of i.r. ozone bands for the MIPAS space experiment, J. Quant. Spectrosc. Rad. Transf., 59, 405-422, https://doi.org/10.1016/S0022-4073(97)00120-9, 1998.

Mlynczak, M. G. and Drayson, R.: Calculation of infrared limb emission by ozone in the terrestrial middle atmosphere 2. Emission calculations, J. Geophys. Res., 95, 16,513-16,521, https://doi.org/10.1029/JD095iD10p16513, 1990.

Morris, G. A., Kawa, S. R., Douglass, A. R., Schoeberl, M. R., Froidevaux, L., and Waters, J., Low-ozone pockets explained, J. Geophys. Res., 103, 3599-3610, https://doi.org/10.1029/97JD02513, 1998.

Remsberg, E., and Lingenfelser, G.: LIMS Version 6 Level 3 dataset, NASA-TM-2010-216690, available at http://www.sti.nasa.gov (last access: 17 September 2019), 13 pp., 2010.

Remsberg, E. E., Haggard, K. V., and Russell III, J. M., Estimation of synoptic fields of middle atmosphere parameters from Nimbus-7 LIMS profile data, J. Atmos. Ocean. Tech, 7, 689-705, https://doi.org/10.1175/1520-0426(1990)007%3C0689:EOSFOM%3E2.0.CO;2, 1990.

Remsberg, E. E., Gordley, L. L, Marshall, B. T., Thompson, R. E., Burton, J., Bhatt, P., Harvey, V. L., Lingenfelser, G., Natarajan, M.: The Nimbus 7 LIMS version 6 radiance conditioning and temperature retrieval methods and results, J. Quant. Spectros. Rad. Transf., 86, 395-424, doi:10.1016/j.jqsrt.2003.12.007, 2004.

Remsberg, E., Lingenfelser, G., Natarajan, M., Gordley, L., Marshall, B. T., and Thompson, E.: On the quality of the Nimbus 7 LIMS version 6 ozone for studies of the middle atmosphere, J. Quant. Spectros. Rad. Transf., 105, 492-518, doi:10.1016/j.jqsrt.2006.12.005, 2007.

Remsberg, E., et al.: LIMS/Nimbus-7 Level 3 Daily 2 deg Latitude Zonal Fourier Coefficients of O3, NO2, H2O, HNO3, Geopotential Height, and Temperature V006, Version: 006, Goddard Earth Sciences Data and Information Services Center (GES DISC), available at: https://disc.gsfc.nasa.gov/datacollection/LIMSN7L3_006.html (last access: 11 March 2021), 2011.

Remsberg, E., Natarajan, M., Fairlie, T. D., Wargan, K., Pawson, S., Coy, L., Lingenfelser, G., and Kim, G.: On the inclusion of Limb Infrared Monitor of the Stratosphere version 6 ozone in a data assimilation system, J. Geophys. Res., 118, 7982-8000, https://doi.org/10.1002/jgrd.50566, 2013.

Remsberg, E., Harvey, V. L., Krueger, A., and Natarajan, M.: Residual temperature bias effects in stratospheric species distributions from LIMS, Atmos. Meas. Tech., 14, 2185-2199, https://doi.org/10.5194/amt-14-2185-2021, 2021.

Shams, S. B., von Walden, P., Hannigan, J. W., Randel, W. J., Petropavlovskikh, I. V., Butler, A. H., and de la Cámara, A.: Analyzing ozone variations and uncertainties at high latitudes during sudden stratospheric warming events using MERRA-2, Atmos. Chem. Phys. Disc., https://doi.org/10.5194/acp-2021-646, 2021.

Shepherd, T. G., Plummer, D. A., Scinocca, J. F., Hegglin, M. I., Fioletov, V. E., Reader, M. C., Remsberg, E., von Clarmann, T., and Wang, H. J.: Reconciliation of halogen-induced ozone loss with the total-column record, Nature Geoscience, 7, 443-449, doi:10.1038/ngeo2155, 2014.

Siskind, D. E., Coy, L., Espy, P.: Observations of stratospheric warmings and mesospheric coolings by the TIMED SABER instrument, Geophys. Res. Lett. 32, http://doi.org/10.1029/2005GL022399, 2005.

Siskind, D. E., Harvey, V. L., Sassi, F., McCormack, J. P., Randall, C. E., Hervig, M. E., and Bailey, S. M.: Two- and three-dimensional structures of the descent of mesospheric trace constituents after the 2013 sudden stratospheric warming elevated stratopause event, Atmos. Chem. Phys., 21, 14059–14077, https://doi.org/10.5194/acp-21-14059-2021, 2021.

Smith, A. K., Espy, P. J., López-Puertas, M., and Tweedy, O. V., Spatial and temporal structure of the tertiary ozone maximum in the polar winter mesosphere, J. Geophys. Res., 123, 4373-4389, https://doi.org/10.1029/2017JD028030, 2018.

Sofieva, V. F., Szela, M., Tamminen, J., Kyrölä, E., Degenstein, D., Roth, C., Zawada, D., Rozanov, A., Arosio, C., Burrows, J. P., Weber, M., Laeng, A., Stiller, G. P., von Clarmann, T., Froidevaux, L., Livesey, N., van Roozendael, M., and Retscher, C.: Measurement report: regional trends of stratospheric ozone evaluated using the MErged GRIdded Dataset of Ozone Profiles (MEGRIDOP), Atmos. Chem. Phys., 21, 6707–6720, https://doi.org/10.5194/acp-21-6707-2021, 2021.

Solomon, S., Kiehl, J. T., Kerridge, B. J., Remsberg, E. E., and Russell III, J. M.: Evidence for nonlocal thermodynamic equilibrium in the $\nu_3$ mode of mesospheric ozone, J. Geophys. Res., 91, 9865-9876, https://doi.org/10.1029/JD091iD09p09865, 1986.

SPARC, Assessment of Stratospheric Aerosol Properties, L. Thomason and Th. Peter, Ed., WCRP-124, WMO/TD- No. 1295, SPARC Report No. 4, 322 pp., 2006.

SPARC: The SPARC Data Initiative: Assessment of stratospheric trace gas and aerosol climatologies from satellite limb sounders, Hegglin, M. I. and Tegtmeier, S., (Eds.), SPARC Report No. 8, WCRP-5/2017, http://www.sparc-climate.org/publications/sparc-reports/, 2017.

Stolarski, R. S., Douglass, A. R., Remsberg, E. E., Livesey, N. J., and Gille, J. C.: Ozone temperature correlations in the upper stratosphere as a measure of chlorine content, J. Geophys. Res., 117, D10305, https://doi.org/10.1029/2012JD017456. 2012.

Tegtmeier, S., Hegglin, M. I., Anderson, J., Bourassa, A., Brohede, S., Degenstein, D., Froidevaux, L., Fuller, R., Funke, B., Gille, J., Jones, A., Kasai, Y., Krüger, K., Kyrölä, E., Lingenfelser, G., Lumpe, J., Nardi, B., Neu, J., Pendlebury, D., Remsberg, E., Rozanov, A.,

https://doi.org/10.5194/amt-2021-340
Preprint. Discussion started: 9 November 2021



688 Smith, L., Toohey, M., Urban, J., von Clarmann, T., Walker, K. A. and Wang, R. H. H.: SPARC Data Initiative: A comparison of ozone climatologies from international satellite limb sounders, J. Geophys. Res., 118, 12,229-12,247, https://doi.org/10.1002/2013JD019877, 2013.

692 WOUDC, World Ozone and Ultraviolet Radiation Data Centre, https://woudc.org/home.php.